High-bandwidth radio frequency Coulter counter

D. K. Wood
Department of Physics and Institute for Collaborative Biotechnologies, University of California at Santa Barbara, Santa Barbara, California 93106

S.-H. Oh and S.-H. Lee
California Nanosystems Institute, University of California at Santa Barbara, Santa Barbara, California 93106

H. T. Soh
Department of Mechanical Engineering and Institute for Collaborative Biotechnologies, University of California at Santa Barbara, Santa Barbara, California 93106

A. N. Cleland[a)]
Department of Physics, University of California at Santa Barbara, Santa Barbara, California 93106

We demonstrate a method for high-bandwidth, high-sensitivity particle sensing and cell counting in a microfluidic system. Our approach employs a tuned radiofrequency probe, which forms the radiofrequency analog of a Coulter counter. By measuring the reflected rf power, this approach provides an unprecedented detection rate, with a theoretical bandwidth in excess of 10 MHz. Particle detection was performed in a continuous flow mode in a microfluidic channel, using 15 μm diameter polystyrene beads suspended in a sucrose-saline solution. We demonstrate 30 kHz counting rates and show high-resolution bead time-of-flight data, comprising the fastest electronic particle detection on-chip to date. © *2005 American Institute of Physics*. [DOI: 10.1063/1.2125111]

High throughput cell counting and analysis is an important biotechnological capability. Since the invention of the Coulter counter,[1] electronic means to count and analyze biological cells have become an essential tool in hematology and oncology. In most implementations of the Coulter counter, the size and concentrations of cells are analyzed in real time, by monitoring the resistance changes in a narrow constriction. Recent advances in microfluidics offer an interesting platform on which disposable, high resolution, high-throughput cell counters may be fabricated, and such devices are presently under development by a number of groups.[2–6] In particular, several groups have investigated electronic techniques, albeit with somewhat limited sensitivity and throughput.[3,7–9]

Achieving large electrical bandwidth in a microfluidic system presents challenges, due to the combination of high electrical impedance, presented by the small volume of ionic solution, with the inevitable stray capacitance of the sensing cabling. The effect of the stray capacitance can be eliminated through the use of a radio frequency (rf) resonance detection technique,[10–12] where the stray capacitance is cancelled by a tank circuit inductance. This approach also achieves better rf impedance match to the sample volume, without sacrificing measurement bandwidth. Using this technique, we have achieved approximately $100\times$ the throughput reported for other electronic detection schemes,[3] and we demonstrate the technique in a microfluidic "flow mode" that allows continuous measurement.

The microfluidic devices with integrated rf electrodes are made using standard optical lithographic techniques. The microfluidic channels are fabricated in polydimethyl siloxane[13] (PDMS) using a silicon mold.[14] The rf electrodes are implemented using optically patterned, thermally evaporated gold/titanium films (500 nm/10 nm thick) on glass chips. Microfluidic connections are formed by drilling holes through the glass chips, and the chips are then aligned and bonded to the PDMS microchannel using a flip-chip bonder. The fluid connections are completed by fixing brass tubes to the chips with epoxy. A photograph of one device is shown in Fig. 1(a). The microchannels are 40 μm deep and either 50 or 200 μm wide. The electrode geometry is a ground-signal-ground coplanar stripline, where in the microchannel the signal electrode is 20 μm wide, the ground-signal spacing is 20 μm, and the ground electrodes are 40 μm wide [Fig. 1(b)]. The microwave stripline widens gradually from the region in the microchannel to the edge of the chip [Fig. 1(a)], where the strip width is made larger to accommodate soldering to a short length of stripline patterned on printed circuit board (PCB). The other end of the PCB stripline is soldered to a subminiature connector.
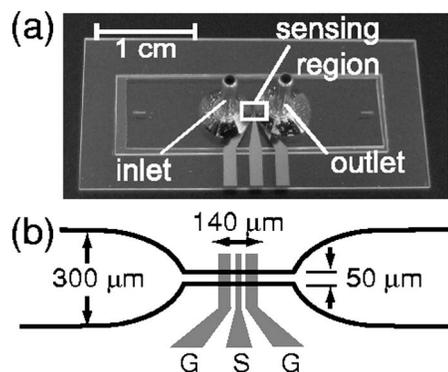

FIG. 1. (a) Photograph of finished device, with fluidic connections. The sensing region is sketched in expanded form in (b), showing 50-μm-wide fluidic channel with integrated coplanar rf electrodes.

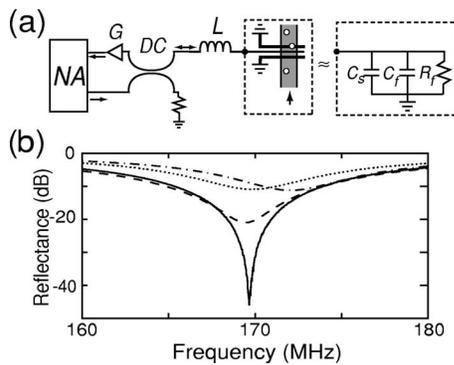[a)]Author to whom correspondence should be addressed; electronic mail: cleland@physics.ucsb.edu

FIG. 2. (a) Circuit schematic; *NA* is a network analyzer, *G* a low-noise amplifier, and *DC* a directional coupler. The microchannel is shown schematically in the left dashed box, and its lumped element representation shown in the right dashed box. (b) Resonance curve with different solutions in the microchannel. Solid curve: $1\times$PSB with 0.168 g/ml sucrose; dashed curve: $1\times$PSB; dotted line: de-ionized water; dot-dashed curve: dry microchannel.

FIG. 3. Time-of-flight data for 15 μm beads flowing at (a) 10, (b) 30, and (c) 50 μl/h. Dashed vertical bars indicate peak-to-peak transit times, which correspond to a distance of 40 μm.

The electrical impedance of the microwave stripline and fluid in the microchannel can be modeled by a parallel resistor-capacitor circuit [Fig. 2(a)], which includes a stray capacitance C_s and the resistance and capacitance of the fluid, R_f and C_f. We connected an inductor L in series with this load, forming a tank circuit with the load capacitance $C=C_s+C_f$, resonant at the frequency $f_c=1/2\pi\sqrt{LC}$; at this frequency, the impedance of the circuit is purely resistive. With the appropriate inductance value, this resistive load can be made equal to the 50 Ω source impedance, and in addition achieves a measurement bandwidth Δf of order 10%–20% of the resonant frequency.[11] In Fig. 2(b) we show the reflection coefficient $S_1(f)$ measured for a fixed inductance and different fluids in the microchannel, using an inductance $L=470$ nH. This yields a resonance frequency $f_c=169$ MHz when the microchannel is filled with $1\times$ concentration standard phosphate buffered saline[15] (PBS), to which we added 0.168 g/ml sucrose to achieve solution isodensity with polystyrene beads (see below). With an on-resonance reflectance $S_1<-45$ dB, this circuit is very well impedance matched and is thus sensitive to small changes in the load impedance, both resistive and capacitive. Removing the sucrose from the PBS (dashed curve) changes the reflectance dramatically, as does replacing the solution with de-ionized water (dotted curve) or air (dot-dashed curve). The bandwidth $\Delta f\approx25$ MHz with the PBS-sucrose solution allows detection of signals with duration as short as 80 ns, which translates to a counting rate as high as 12 million particles (e.g., beads or biological cells) per second.

Following characterization of the rf properties of the sensor, we added a suspension of 15-μm-diam polystyrene beads to the solution.[16] The beads and solution were designed to be at isodensity to prevent settling. We then operated the device as a radio frequency Coulter counter by monitoring the time-dependent reflection $S_1(t)$ as beads flowed through the microchannel. We measured S_1 at the resonance frequency of the device.

As the beads in the microchannel flow past the electrodes, they alter the effective impedance of the heterogeneous fluid mixture, modulating the probe reflectance S_1. On resonance, most of the power is absorbed by the fluid, making this a dark field measurement, with high contrast for small signals. Measurements were carried out with the circuit
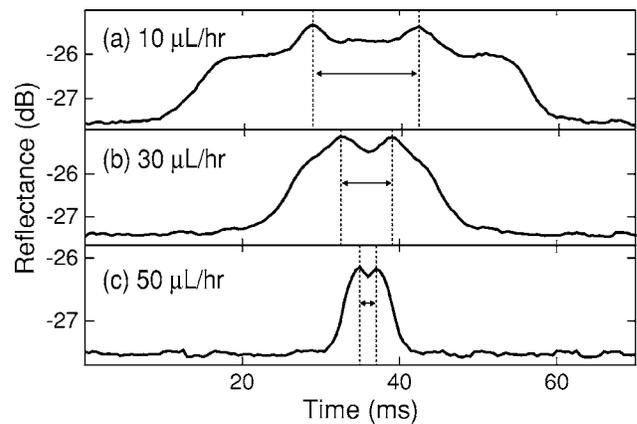
shown in Fig. 2(a), using an injected power that corresponds to about 30 μW absorbed in the fluid, which causes a temperature change of at most 2.5 °C in the ionic solution at a flow rate of 10 μl/h. Reflected power was amplified by a room temperature rf amplifier.

Flow through the microchannel was controlled using a syringe pump[17] while monitoring the reflectance signal. Signals were correlated by visual inspection and video monitoring through an optical microscope. Because of the high temporal resolution of our device, we were able to perform time-of-flight measurements for individual beads using a single set of electrodes. Figure 3 shows time-domain data for 15 μm beads flowing through a 50×40 μm^2 cross-section channel at 10, 30 and 50 μl/h. The observed signals are large, with a 1–2 dB change in the signal as a bead passes through the electrode volume. Some variation is seen due to difference in the bead position in the channel, as reported by Gawad, Schild, and Renaud.[7]

The detailed shape of the curves in Fig. 3 corresponds to onset as the bead crosses the first ground electrode, two peaks as the bead crosses the region between the signal and two ground electrodes, and decaying as the bead passes the second ground electrode. The regions between the signal and two ground electrodes are those with the highest electrical field, so the two peaks in the response correspond to when the beads are passing through these regions. Hence the peak-to-peak traversal time corresponds to the midpoint-to-midpoint distance of 40 μm, from which we can extract the bead velocity. The beads in Figs. 3(a)–3(c) give peak-to-peak transit times of 14, ms 6.3, ms and 2.4 ms respectively, which correspond to bead velocities of 2.9, 6.4, and 17 mm/s. A flow rate of 10 μl/h in this channel corresponds to a theoretical maximum channel velocity of 2.9 mm/s and a transit time of 14 ms.[18] Similarly, we expect transit times and velocities of 4.6 ms (8.7 mm/s) and 2.8 ms (15 mm/s) for the 30 and 50 μl/h flow rates, respectively. The measured bead velocity varies from bead to bead depending on the bead location in the channel, and is typically smaller but close to that expected.

We then performed measurements at longer time scales to extract bead count rates as a function of flow rate. In Fig. 4(a) we show the time-dependent reflection for 15 μm beads at a concentration of 46 beads/μl flowing at 100 μl/h through a 50×40 μm^2 channel, corresponding to a maxi-
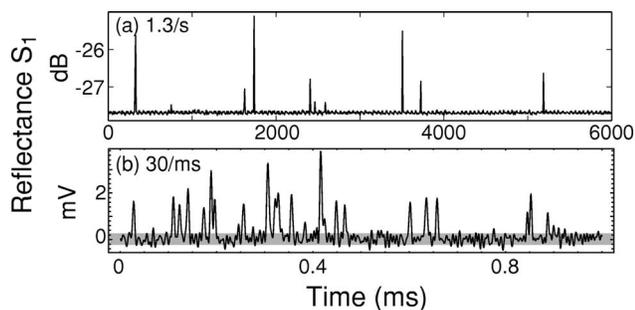
FIG. 4. RF reflectance data taken for 15 μm beads (a) flowing at 1.3 beads/s and (b) flowing at 30 000 beads/s. Note the horizontal and vertical scales are different. The gray bar indicates the noise level for (b). Data in (b) are at output of amplifier-mixer combination, with a combined voltage gain of 32×.

mum flow velocity of 30 mm/s and a transit time of about 1.3 ms. The peaks in S_1 are again very distinct, with variations in peak height corresponding to variations in bead position in the channel. This variation appears because the electrode geometry concentrates the electric field close to the electrode plane, so that the signals are smaller for beads further from the electrode plane. A finite-element reconstruction of the electric field, using the experimental geometry and saline concentration, shows that the field falls approximately linearly with height z above the electrode plane, up to the electrode spacing of 20 μm, where it has about 40% its value at $z=0$. Above this point, the field strength has a roughly $1/z$ dependence. This monotonic dependence will be reflected in the signal amplitude, yielding a possible direct measurement of bead height.

The flow rate in Fig. 4(a) corresponds to 1.3 beads/s, and is close to the measured rate of 1.4/s. We then greatly increased the flow rate, and measured at a calculated rate of 30 000 beads/s. For this measurement we used a homodyne mixer to demodulate the rf signal, which was then amplified by a 1 MHz bandwidth amplifier, and flowed the beads through a 200×40 μm^2 channel. After digital filtering the measurement bandwidth was 175 kHz. In Fig. 4(b) we show a typical data trace captured with this arrangement. The bead count rate of 25/ms is close to the calculated value of 30/ms. This rate is roughly 100× that reported for other electronic detection schemes,[3] and is comparable to that of commercial fluorescence activated cell sorters.[19]

The limit for bead detection ultimately will be set by the signal to noise ratio (S/N), which is reduced as the measurement bandwidth is increased to follow the count rate. Higher signal powers yield a better S/N, as does the use of low-noise amplifiers. The width of the gray box in Fig. 4(b) corresponds to a noise level of 26 nV/$\sqrt{\text{Hz}}$ referenced to the amplifier input, and with the digital bandwidth of 175 kHz

yields a S/N ratio of about 4; smaller values will yield poor counting statistics. The noise level for the setup is dominated by the rf electronics.

In conclusion, we have demonstrated the use of a tuned rf circuit as a microchannel Coulter counter. Our implementation has an intrinsic bandwidth in excess of 10 MHz, allowing count rates approaching millions of beads, or cells, per second. We have shown measurement of 15 μm polystyrene beads at different rates, demonstrating both time-of-fight and high flow rate measurements, up to 30 kHz. This technique, with its intrinsically high throughput and sensitivity, could play a significant role in the future development of electrically based microfluidic systems for disposable cellular analysis.

[1]W. H. Coulter, U. S. Patent No. 2,656,508 (1953).
[2]A. G. Tibbe, B. G. de Grooth, J. Greve, G. J. Dolan, C. Rao, and L. W. Terstappen, Cytometry **47**, 163 (2002).
[3]S. Gawad, K. Cheung, U. Seger, A. Bertsch, and P. Renaud, Lab Chip **4**, 241 (2004).
[4]M. Berger, J. Castelino, R. Huang, M. Shah, and R. H. Austin, Electrophoresis **22**, 3883 (2001).
[5]M. Dürr, J. Kentsch, T. Müller, T. Schnelle, and M. Stelzle, Electrophoresis **24**, 722 (2003).
[6]M. M. Wang, E. Tu, D. E. Raymond, J. M. Yang, H. Zhang, N. Hagen, B. Dees, E. M. Mercer, A. H. Forster, P. J. Marchand, and W. F. Butler, Nat. Biotechnol. **23**, 83 (2005).
[7]S. Gawad, L. Schild, and P. Renaud, Lab Chip **1**, 76 (2001).
[8]L. L. Sohn, O. A. Saleh, G. R. Facer, A. J. Beavis, R. S. Allan, and D. A. Notterman, PNAS **97**, 10687 (2000).
[9]G. R. Facer, D. A. Notterman, and L. L. Sohn, Appl. Phys. Lett. **78**, 996 (2001).
[10]R. J. Schoelkopf, P. Wahlgren, A. A. Kozhevnikov, P. Delsing, and D. E. Prober, Science **280**, 1238 (1998).
[11]D. R. Schmidt, C. S. Yung, and A. N. Cleland, Appl. Phys. Lett. **83**, 1002 (2003).
[12]D. R. Schmidt, C. S. Yung, and A. N. Cleland, Phys. Rev. B **69**, 140301 (2004).
[13]*Sylgard 184*, Dow-Corning Inc.
[14]Y. Xia, E. Kim, X.-M. Zhao, J. A. Rogers, M. Prentiss, and G. M. Whitesides, Science **273**, 347 (1996).
[15]Phosphate buffered saline concentrate, Sigma-Aldrich Co. Working 1× solution contains 10 mM sodium phosphate and 0.9 wt% sodium chloride in water.
[16]Bangs Laboratories, Inc., Fishers, IN.
[17]Harvard Apparatus, Holliston, MA.
[18]M. Spiga and G. L. Morino, Int. Commun. Heat Mass Transfer **21**, 469 (1994).
[19]S. F. Ibrahim and G. van den Engh, Curr. Opin. Biotechnol. **14**, 5 (2003).